Iranian Journal of Mathematical chemistry

IJMC

DOI: 10.22052/ijmc.2026.257981.2091
Vol. 17, No. 3, 2026, pp. 233-253
Research Paper

Concentration of Ethanol and Acetaldehyde Inside the Catalyst Particle and in the Reaction Stream: Theoretical and Numerical Approach

Baskaran Yamuna[1], Athimoolam Meena[1], Lakshmanan Rajendran[2] and Mohammad Izadi[3,4*]

[1]Department of Mathematics, Saraswathi Narayanan College, Madurai-625022, India
[2]Department of Mathematics, AMET Deemed to be University, Kanathur, Chennai- 603112, India
[3]Department of Applied Mathematics, Faculty of Mathematics and Computer, Shahid Bahonar University of Kerman, Kerman 76169-14111, Iran
[4]Department of Mathematics, Saveetha School of Engineering, SIMATS, Saveetha University, Chennai 602105, Tamil Nadu, India

Keywords:
Catalytic combustion
Nonlinear reaction kinetics
Fixed-bed reactor modelling
Hyperbolic function method
Mathematical chemistry

AMS Subject Classification (2020):
34K25; 35K57; 80A30

Article History:
Received: 17 November 2025,
Accepted: 14 March 2026

Abstract

The current research investigates the nonlinear behaviour of dimensionless ethanol and acetaldehyde concentrations in a fixed-bed laboratory reactor operating with a Mn_9Cu_1 catalyst for catalytic combustion. The main objective is to obtain accurate analytical solutions of the coupled nonlinear governing equations and evaluate their usefulness for reactor analysis. A semi-analytical hyperbolic function method is applied to derive rapidly convergent solutions, which are validated through MATLAB (version 7.8.0, R2009a) numerical simulations. Excellent agreement between analytical and numerical results confirms the reliability of the method. The findings show that the approach efficiently captures reactive transport and catalytic kinetics while reducing computational iteration time. The solutions provide insight into catalyst performance and ethanol oxidation efficiency, supporting optimization of reactor operating conditions. Overall, the study demonstrates that the hyperbolic function method is a simple, computationally efficient tool for modelling complex nonlinear catalytic combustion systems.

*Corresponding author
E-mail addresses: yamunabaskaran17797@gmail.com (B. Yamuna), meensphd@gmail.com (A. Meena), dr.rajendran.l@gmail.com (L. Rajendran), izadi@uk.ac.ir (M. Izadi)
Academic Editor: Abbas Saadatmandi

1 Introduction

Ethanol combustion has become a focal point in environmental remediation efforts owing to its significance in the abatement of volatile organic compounds (VOCs) emanating from industrial effluents, particularly in manufacturing sectors such as printing and chemical processing. VOCs are a major contributor to air pollution, playing a role in both indoor and outdoor air quality degradation, photochemical smog formation, and posing notable health risks [1–3]. Innovative treatment methods, especially catalytic combustion, have emerged as vital solutions for managing VOC emissions, enabling efficient oxidation at reduced temperatures and minimizing the release of hazardous byproducts [4, 5].

Among the catalysts explored for ethanol combustion, manganese-copper mixed oxides have demonstrated superior catalytic activity, stability, and selectivity, making them promising candidates for the complete oxidation of VOCs [6–9]. Recent advances focus on the development of robust kinetic models and optimization of reaction parameters for these catalysts, including the novel Mn_9Cu_1 composition [8, 10]. Such models are pivotal for enhancing industrial reactor designs and maximizing combustion efficiency, as they integrate experimental findings with advanced modelling approaches [8, 11, 12].

Catalyst composition has a profound impact on reaction pathways, the formation of intermediate species, and the overall catalytic performance [13]. The integration of experimental kinetic studies with predictive models advances the understanding of catalytic combustion for VOC control, supporting the development of tailored strategies for industrial emission management [9, 14, 15]. This body of work underscores the multidisciplinary effort required for effective environmental protection and industrial process optimization in the context of ethanol-based VOC abatement.

Various researchers [16–23] have contributed extensively to the development of analytical and semi-analytical methods for nonlinear differential equations. Their studies address a wide range of nonlinear evolution models arising in mathematical physics and engineering. These works provide accurate solution structures and valuable insights into complex nonlinear phenomena. The authors in [24] studied the transcendental Bernstein series method for reaction–diffusion equations with nonlocal boundary conditions, using optimization techniques to enhance accuracy and convergence. In their subsequent works, they proposed efficient numerical and semi-analytical approaches, including generalized Bernoulli–Laguerre polynomials and Lagrange scaling functions, to address a broad class of nonlinear differential equations in applied sciences and engineering [25–27]. More recently, these methods have been successfully extended to coupled nonlinear systems of variable-order fractional PDEs and time-fractional convection–diffusion–wave equations, demonstrating their versatility and robustness in handling complex physical phenomena [25, 27]. Further advancements in this domain include the application of reproducing kernel methods for nonlinear singular boundary value problems [28], as well as analytical and semi-analytical solutions for time-dependent chemical reaction–diffusion systems, such as the glycolysis model [29] and transient electrochemical processes at spherical microelectrodes [30]. These contributions underscore the growing utility of hybrid numerical techniques in modeling complex nonlinear phenomena across chemistry, biology, and electrochemistry.

A nonlinear coupled diffusion–reaction model describes ethanol and acetaldehyde transport inside porous catalyst pellets, using the Bosanquet model for diffusivity and nonlinear kinetics for the ethanol-to-acetaldehyde pathway. In this communication, we have derived the analytical expression of concentration of ethanol and acetaldehyde using the hyperbolic function method (HFM). This method provides efficient analytical solutions, validated against numerical results, supporting mechanistic insight and practical catalyst or reactor optimization in

complex reaction–diffusion systems. Parametric studies reveal impacts of key dimensionless groups on system behaviour. HFM outperforms variational iteration method (VIM) and the Adomian decomposition method (ADM) by delivering exact closed-form soliton solutions (e.g., sinh/cosh) for nonlinear PDEs with minimal iterations, avoiding infinite series expansions while reducing computational effort in reaction-diffusion modelling.

2 Mathematical formulation

2.1 Molar concentrations of ethanol and acetaldehyde inside the catalyst particle

In the study by Agustina Campesi et al. [31], a mathematical model was proposed to describe the molar concentrations of ethanol and acetaldehyde within a catalyst particle. The experimental model considers ethanol oxidation on a catalyst, proceeding via consecutive reactions: ethanol forms acetaldehyde, which is then oxidized to $CO2$ and $H2O$. The process is described by Langmuir–Hinshelwood–Hougen–Watson kinetics, with reaction rates dependent on ethanol and acetaldehyde concentrations.

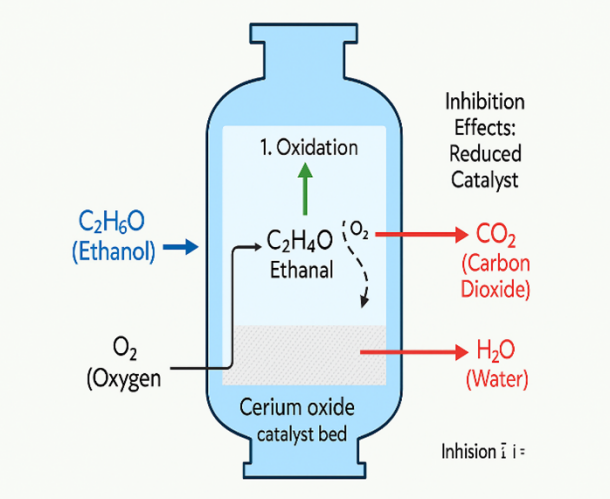

Figure 1: Schematic diagram of ethanol oxidation and intermediate formation over cerium oxide catalyst bed.

Figure 1 illustrates the oxidation pathway of ethanol over a cerium oxide catalyst, highlighting key reactants, products, and inhibition effects. The key chemical equations are:

$$\left.\begin{aligned} \mathrm{C_2H_6O} + \left(\frac{1}{2}\right)\mathrm{O_2} &\rightarrow \mathrm{C_2H_4O} + \mathrm{H_2O} \\ \mathrm{C_2H_4O} + \left(\frac{5}{2}\right)\mathrm{O_2} &\rightarrow 2\mathrm{CO_2} + 2\mathrm{H_2O} \end{aligned}\right\}. \tag{1}$$

This model is governed by nonlinear differential equations. The system of equations is given as:

$$\begin{cases} D_{ef,Et}\left[\frac{d^2C_{Et}(z)}{dz^2} + \frac{2}{z}\frac{dC_{Et}(z)}{dz}\right] = r_1\left(C_{Et}, C_{Ac}\right), \\ D_{ef,Ac}\left[\frac{d^2C_{Ac}(z)}{dz^2} + \frac{2}{z}\frac{dC_{Ac}(z)}{dz}\right] = r_2\left(C_{Et}, C_{Ac}\right) - r_1\left(C_{Et}, C_{Ac}\right). \end{cases} \tag{2}$$

The boundary conditions for these equations are:

$$C_{Et} = C_{Et}^b, \quad C_{Ac} = C_{Ac}^b \quad \text{at} \quad z = R, \tag{3}$$

$$\frac{dC_{Et}}{dz} = \frac{dC_{Ac}}{dz} = 0 \quad \text{at} \quad z = 0. \tag{4}$$

The reaction rates r_1 and r_2 are expressed as:

$$\begin{pmatrix} r_1\left(C_{Et}, C_{Ac}\right) \\ r_2\left(C_{Et}, C_{Ac}\right) \end{pmatrix} = \begin{pmatrix} k_{ref,1} \exp\left[-\dfrac{E_1}{R_G}\left(\dfrac{1}{T} - \dfrac{1}{T_{ref}}\right)\right] \dfrac{C_{Et}}{1 + K_{C_{Et}} C_{Et} + K_{C_{Ac}} C_{Ac}} \\ k_{ref,2} \exp\left[-\dfrac{E_2}{R_G}\left(\dfrac{1}{T} - \dfrac{1}{T_{ref}}\right)\right] \dfrac{K_{C_{Ac}} C_{Ac}}{1 + K_{C_{Et}} C_{Et} + K_{C_{Ac}} C_{Ac}} \end{pmatrix}. \tag{5}$$

This compact vector form combines both kinetic expressions for the system, clearly representing the nonlinear Arrhenius-Michaelis -Menten dependence on concentrations and temperature. Here, C_{Et} and C_{Ac} represent the molar concentrations of ethanol and acetaldehyde inside the catalyst particle, respectively, while $D_{\text{ef},Et}$ and $D_{\text{ef},Ac}$ denote their corresponding effective diffusivities. R is the radius of the catalyst particle, and T is the operating temperature, with T_{ref} serving as the reference temperature. R_G stands for the universal gas constant. $K_{C_{Et}}$ and $K_{C_{Ac}}$ are the adsorption equilibrium constants for ethanol and acetaldehyde, respectively, and E_1 and E_2 are the activation energies associated with the respective reactions or adsorption processes.

To nondimensionalize the system, the following substitutions are introduced:

$$\begin{cases} U = \frac{C_{Et}}{C_{Et}^b},\ W = \frac{C_{Ac}}{C_{Ac}^b},\ x = \frac{z}{R},\ \phi_1^2 = \frac{k_{ref,1} R^2}{D_{ef,Et}},\ \phi_2^2 = \frac{k_{ref,2} R^2}{D_{ef,Et}},\ \phi_3^2 = \frac{k_{ref,1} C_{Et}^b R^2}{D_{ef,Ac} C_{Ac}^b}, \\ \beta_1 = K_{C_{Et}} C_{Et}^b,\ \beta_2 = K_{C_{Ac}} C_{Ac}^b,\ \gamma_1 = \frac{E_1}{R_G}\left(\frac{1}{T} - \frac{1}{T_{ref}}\right),\ \gamma_2 = \frac{E_2}{R_G}\left(\frac{1}{T} - \frac{1}{T_{ref}}\right). \end{cases} \tag{6}$$

Using these dimensionless variables (6), Equations in (2) transform into a coupled system of nonlinear ODEs:

$$U''(x) + \frac{2}{x} U'(x) = \phi_1^2 e^{-\gamma_1} f_1(U(x), W(x)), \tag{7}$$

$$W''(x) + \frac{2}{x} W'(x) = \phi_2^2 e^{-\gamma_2} f_2(U(x), W(x)) - \phi_3^2 e^{-\gamma_1} f_1(U(x), W(x)), \tag{8}$$

with boundary conditions:

$$\text{At} \quad x = 0: \quad \frac{dU}{dx} = 0, \quad \frac{dW}{dx} = 0, \tag{9}$$

$$\text{At} \quad x = 1: \quad U = 1, \quad W = 1. \tag{10}$$

Here, $U(x)$ and $W(x)$ denote the dimensionless concentrations of ethanol and acetaldehyde, respectively, and x is the dimensionless axial position inside the catalyst particle. Here, we have:

$$f_1(U, W) = \frac{U(x)}{1 + \beta_1 U(x) + \beta_2 W(x)}, \quad f_2(U, W) = \frac{W(x)}{1 + \beta_1 U(x) + \beta_2 W(x)}. \tag{11}$$

3 Approximation of molar concentrations of ethanol and acetaldehyde inside the catalyst particle using the HFM

The HFM is a powerful technique for solving nonlinear differential equations. By substituting this assumed form into the differential equation, the method transforms the problem into

an algebraic system for determining unknown coefficients. HFM efficiently handles boundary and initial conditions, providing accurate analytical solutions with fewer computational steps. Compared to other methods, HFM is particularly effective for problems involving boundary layers and steep gradients. For detailed applications of the HFM, see [32–34]. Using the HFM, analytical expressions for the reactant concentrations are obtained from the governing dimensionless Equations (7) and (8) over the specified parameter range. The detailed HFM solution procedure is illustrated in Appendix A and Figure 7. Let

$$U(x) = \frac{\cosh(mx)}{\cosh(m)}, \tag{12}$$

$$W(x) = \frac{\cosh(nx)}{\cosh(n)}, \tag{13}$$

where m and n are obtained by solving the following equations:

$$\frac{3m^2}{\cosh(m)} = \frac{\phi_1^2 e^{-\gamma_1}\cosh(n)}{\cosh(n)\left(\cosh(m)+\beta_1\right)+\beta_2\cosh(m)}, \tag{14}$$

$$\frac{3n^2}{\cosh(n)} = \left(\frac{\phi_2^2 e^{-\gamma_2}\cosh(m)-\phi_3^2 e^{-\gamma_1}\cosh(n)}{\cosh(n)\left(\cosh(m)+\beta_1\right)+\beta_2\cosh(m)}\right). \tag{15}$$

The numerical values of $m$and n for specified values of $\phi_1^2, \phi_2^2, \phi_3^2, \gamma_1, \gamma_2, \beta_1, \beta_2$ can be computed using mathematical software such as Wolfram Alpha.

When m and n are small, the hyperbolic functions in Equations (14) and (15) are expanded using Taylor series, namely $\cosh(m) \approx 1 + m^2/2$ and $\cosh(n) \approx 1 + n^2/2$. Substituting these expansions into the governing algebraic equations and neglecting higher-order terms $O\left(m^4, n^4\right)$ yield the reduced expressions for m^2 and n^2 presented in Equations (16) and (17). These approximations are valid in the small-parameter regime.

$$m^2 = \frac{\phi_1^2\left(1-\gamma_1\right)}{3\left(1+\beta_1+\beta_2\right)}\left[1+\frac{n^2\beta_2}{2\left(1+\beta_1+\beta_2\right)}\right], \tag{16}$$

$$3n^2 \approx \frac{\phi_2^2\left(1-\gamma_2+\frac{m^2}{2}\left(1-\gamma_2\right)\right)-\phi_3^2\left(1-\gamma_1+\frac{n^2}{2}\left(1-\gamma_1\right)\right)}{1+\beta_1+\beta_2+\frac{m^2}{2}\left(1+\beta_2\right)+\frac{n^2}{2}\left(1+\beta_1\right)}. \tag{17}$$

4 Previous analytical results

Equations (7) and (8), along with the boundary conditions (9) and (10), were previously solved by Dharmalingam et al. used both the ADM [35] and the VIM [36]. Their study provided the molar concentration profiles of ethanol and acetaldehyde, as shown below:

4.1 VIM

Dharmalingam et al. [36] have recently derived the analytical expressions for reactant concentrations using VIM as follows:

$$\begin{cases} U(x) = 2\delta + \left(\dfrac{\phi_1^2 e^{-\gamma_1}\delta}{1+\beta_1\delta+\beta_2\delta'}\right)\frac{x^2}{6}, \\ W(x) = 2\delta' + \left(\dfrac{\phi_2^2 e^{-\gamma_2}\delta' - \phi_3^2 e^{-\gamma_1}\delta}{1+\beta_1\delta+\beta_2\delta'}\right)\frac{x^2}{6}, \end{cases} \tag{18}$$

where the constants δ and δ' are obtained by using the boundary conditions $U(1) = 1$ and $W(1) = 1$.

The VIM suffers from repeated and unnecessary computations at each step, making it inefficient for complex problems. It can also struggle with slow convergence if Lagrange multipliers are not selected accurately and may not easily handle highly nonlinear or stiff problems.

4.2 ADM

Dharmalingam et al. [35] recently derived analytical expressions for the reactant concentrations using the ADM as follows:

$$\begin{cases} U(x) = 1 + \dfrac{\phi_1^2 e^{-\gamma_1}}{6\,(1+\beta_1+\beta_2)}\left(x^2-1\right), \\ W(x) = 1 + \dfrac{\phi_2^2 e^{-\gamma_2} - \phi_3^2 e^{-\gamma_1}}{6\,(1+\beta_1+\beta_2)}\left(x^2-1\right). \end{cases} \tag{19}$$

The ADM offers analytic solutions without linearization or perturbation but has drawbacks. It produces series solutions that require truncation, potentially limiting accuracy and the convergence region. Slow convergence and sensitivity to initial approximations can restrict its applicability, especially for complex nonlinear problems.

5 Validation of results

Model validation was performed using Figures 2 to 6 and Tables 1 to 3, which illustrate the concentration profiles of ethanol and acetaldehyde inside the catalyst particle. The results show an excellent agreement between the analytical solutions and numerical simulations (Matlab), confirming the model's reliability. The Matlab program (version 7.8.0, R2009a) is also given in Appendix B. Notably, average deviations calculated from the tables highlight the superior accuracy of the HFM (this work) method with an average deviation of only 0.0138, compared to 0.1501 for the VIM approach and 0.1676 for ADM approach. These findings demonstrate the robustness of the proposed methodology for accurately predicting concentration distributions, supporting its utility for catalytic process analysis and design. The graphs demonstrate the

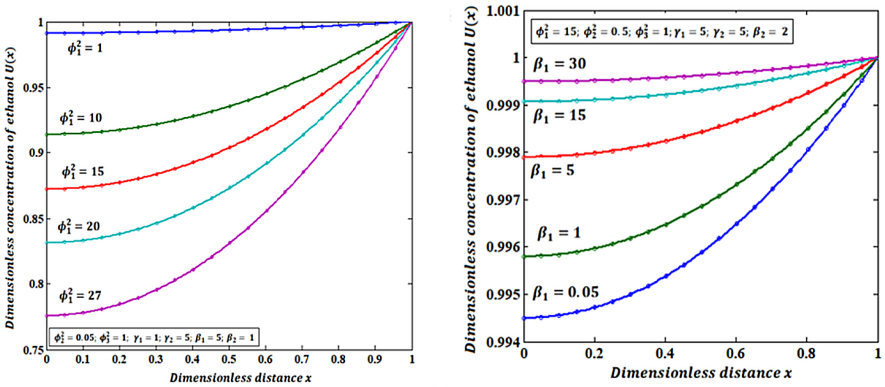

Figure 2: Comparison of numerical (dotted line) and analytical (solid line) results of the dimensionless concentration of ethanol $U(x)$ on the effect of ϕ_1^2 and β_1.

Table 1: Comparison between numerical and analytical results for the dimensionless concentration $U(x)$ for various values of parameters.

x	$\phi_1^2 = 15; \phi_2^2 = 0.05; \phi_3^2 = 1; \gamma_1 = 1; \gamma_2 = 5; \beta_1 = 5; \beta_2 = 1,$ $m = 0.53808$							$\phi_1^2 = 10; \phi_2^2 = 1; \phi_3^2 = 1; \gamma_1 = 1; \gamma_2 = 1; \beta_1 = 0.01; \beta_2 = 0.1,$						
	Num	HFM (This work) Eq. (12)	Deviation (HFM)	VIM [36] Eq. (18)	Deviation (VIM)	ADM [35] Eq. (19)	Deviation (ADM)	Num	HFM (This work) Eq. (12)	Deviation (HFM)	VIM [36] Eq. (18)	Deviation (VIM)	ADM [35] Eq. (19)	Deviation (ADM)
0.0	0.8724	0.8709	0.0015	0.8902	0.0178	0.8687	0.0037	0.6046	0.6217	0.0171	0.7746	0.1700	0.4476	0.1570
0.2	0.8774	0.8760	0.0014	0.8951	0.0177	0.8740	0.0034	0.6182	0.6357	0.0175	0.7837	0.1655	0.4697	0.1485
0.4	0.8925	0.8911	0.0014	0.9091	0.0166	0.8897	0.0028	0.6603	0.6783	0.0180	0.8110	0.1507	0.5360	0.1243
0.6	0.9179	0.9166	0.0013	0.9323	0.0144	0.9160	0.0019	0.7341	0.7515	0.0174	0.8566	0.1225	0.6465	0.0876
0.8	0.9537	0.9528	0.0009	0.9647	0.0110	0.9527	0.0010	0.8459	0.8584	0.0125	0.9203	0.0744	0.8011	0.0448
1.0	1.0000	1.0000	0.0000	0.9999	0.0001	1.0000	0.0000	1.0000	1.0000	0.0000	1.0000	0.0000	1.0000	0.0000
Mean Deviation			0.0011		0.0129		0.0021			0.0138		0.1139		0.0937

Table 2: Comparison between numerical and analytical results for the dimensionless concentration $W(x)$ for various values of parameters.

x	$\phi_1^2 = 0.8; \phi_2^2 = 3; \phi_3^2 = 5; \gamma_1 = 5; \gamma_2 = 0.5; \beta_1 = 0.1; \beta_2 = 2$													
x	Num	HFM (This work) Eq. (12)	Deviation (HFM)	VIM [36] Eq. (18)	Deviation (VIM)	ADM [35] Eq. (19)	Deviation (ADM)	Num	HFM (This work) Eq. (12)	Deviation (HFM)	VIM [36] Eq. (18)	Deviation (VIM)	ADM [35] Eq. (19)	Deviation (ADM)
0.0	0.3698	0.3780	0.0082	0.5852	0.2154	0.0849	0.2849	0.9065	0.9060	0.0005	0.9302	0.0237	0.9040	0.0025
0.2	0.3900	0.3985	0.0085	0.6020	0.2120	0.1215	0.2685	0.9102	0.9097	0.0005	0.9330	0.0228	0.9078	0.0024
0.4	0.4533	0.4620	0.0087	0.6522	0.1989	0.2313	0.2220	0.9214	0.9210	0.0004	0.9415	0.0201	0.9194	0.0020
0.6	0.5679	0.5754	0.0075	0.7361	0.1682	0.4143	0.1536	0.9402	0.9398	0.0004	0.9556	0.0154	0.9386	0.0016
0.8	0.7471	0.7509	0.0038	0.8533	0.1062	0.6706	0.0765	0.9667	0.9664	0.0003	0.9753	0.0086	0.9654	0.0013
1.0	1.0000	1.0000	0.0000	1.0000	0.0000	1.0000	0.0000	1.0000	1.0000	0.0000	0.9999	0.0001	1.0000	0.0000
Mean Deviation			0.0061		0.1501		0.1676			0.0003		0.0151		0.0016

Table 3: Comparison of the concentration of Ethanol $U(x)$ with the numerical result and the analytical result.

Concentration of Ethanol U(x)															
	$\phi_1^2=1;\phi_2^2=1;\phi_3^2=1;\gamma_2=1;\beta_1=1;$ $\beta_2=1;\gamma_1=5$					$\phi_1^2=1;\phi_2^2=1;\phi_3^2=1;\gamma_2=0.5;\beta_1=1;$ $\beta_2=1;\gamma_1=2.5$					$\phi_1^2=1;\phi_2^2=1;\phi_3^2=1;\gamma_2=1;\beta_1=10;$ $\beta_2=10;\gamma_1=1$				
x	Num	VIM [36] Eq. (18)	Error % (VIM)	HFM (This work) Eq. (12)	Error % (HFM)	Num	VIM [36] Eq. (18)	Error % (VIM)	HFM (This work) Eq. (18)	Error % (HFM)	Num	VIM [36] Eq. (18)	Error % (VIM)	HFM (This work) Eq. (12)	Error % (HFM)
0.0	0.999659	0.999718	0.005902	0.999623	0.003601	0.995435	0.996570	0.114020	0.995496	0.006127	0.997048	0.997218	0.017050	0.997081	0.003309
0.2	0.999643	0.999729	0.008603	0.999638	0.000500	0.995646	0.996707	0.106563	0.995593	0.005323	0.997144	0.997329	0.018553	0.997198	0.005415
0.4	0.999713	0.999763	0.005001	0.999684	0.002901	0.996133	0.997118	0.098882	0.996143	0.001003	0.997567	0.997663	0.009623	0.997548	0.001905
0.6	0.999737	0.999819	0.008202	0.999759	0.002200	0.997128	0.997804	0.067795	0.997061	0.006719	0.998124	0.998219	0.009518	0.998131	0.000701
0.8	0.999855	0.999898	0.004301	0.999864	0.000900	0.998339	0.998765	0.042670	0.998347	0.000801	0.998976	0.998998	0.002202	0.998948	0.002803
1.0	1.000000	0.999999	0.000100	1.000000	0.000000	1.000000	0.999999	0.000100	1.000000	0.000000	1.000000	1.000000	0.000000	1.000000	0.000000
	Average Error %		0.005351		0.001684	Average Error %		0.071672		0.003328	Average Error %		0.009491		0.002355

effects of the parameters ϕ_1^2 and β_1 on the dimensionless ethanol concentration $U(x)$ along the surface. Figure 2(a), an increase in ϕ_1^2 leads to a pronounced decrease in $U(x)$ across the entire domain. Physically, this behavior signifies enhanced resistance to mass diffusion, which may arise due to stronger nanoparticle volume fraction, porous medium resistance, or intensified interaction between the fluid and solid matrix. As a result, ethanol diffusion is suppressed, particularly near the wall region. Conversely, Figure 2(b) reveals that increasing β_1 enhances the ethanol concentration profile. This suggests that higher β_1 values strengthen relaxation, reaction, or diffusion mechanisms, thereby facilitating mass transport and improving ethanol distribution within the boundary layer. Moreover, the smooth convergence of all profiles to the same boundary condition confirms physical consistency. Figure 3 illustrates the effects of the

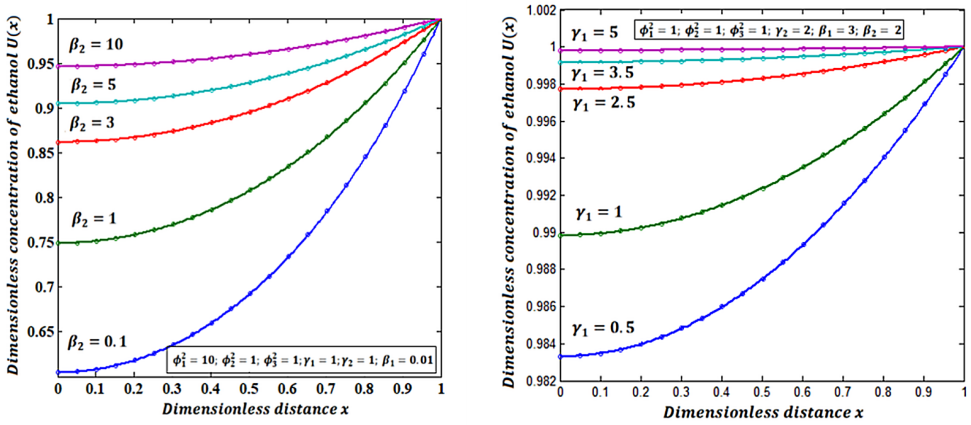

Figure 3: Comparison of numerical (dotted line) and analytical (solid line) results of the dimensionless concentration of ethanol $U(x)$ on the effect of β_2 and γ_1.

parameters β_2 and γ_1 on the dimensionless ethanol concentration $U(x)$. Figure 3(a), an increase in β_2 results in a marked enhancement of $U(x)$ throughout the domain. Physically, this indicates that higher β_2 strengthens the mass diffusion or reaction-related mechanisms, thereby reducing resistance to ethanol transport and promoting higher concentration levels near the surface and within the boundary layer. Conversely, lower β_2 values significantly suppress ethanol concentration, reflecting weaker mass transfer characteristics. Figure 3(b), increasing the parameter γ_1 also elevates the ethanol concentration profile. This behavior suggests that γ_1 enhances the effective diffusivity or chemical activity of ethanol, leading to improved species transport. In both cases, all profiles smoothly satisfy the boundary condition at $x = 1$. Figure 4 depicts the variation of the dimensionless acetaldehyde concentration $W(x)$ under the influence of the parameters ϕ_2^2 and ϕ_3^2. Figure 4(a), increasing ϕ_2^2 causes a significant reduction in $W(x)$ across the entire domain. Physically, this trend indicates that larger values of ϕ_2^2 enhance resistance to species diffusion, which may be attributed to stronger porous medium effects or intensified interaction between acetaldehyde molecules and the surrounding fluid matrix. Consequently, mass transport is suppressed, leading to lower concentration levels near the surface. In contrast, Figure 4(b) shows that increasing ϕ_3^2 results in an increase in acetaldehyde concentration. This behavior suggests that ϕ_3^2 enhances the effective diffusivity or reaction-related transport mechanism, thereby facilitating acetaldehyde diffusion within the boundary layer. In both cases, all concentration profiles smoothly converge to the prescribed boundary condition. Figure 5 presents the influence of the parameters γ_1 and γ_2 on the dimensionless acetaldehyde concentration $W(x)$. Figure 5(a), an increase in γ_1 leads to a noticeable reduction in $W(x)$ throughout

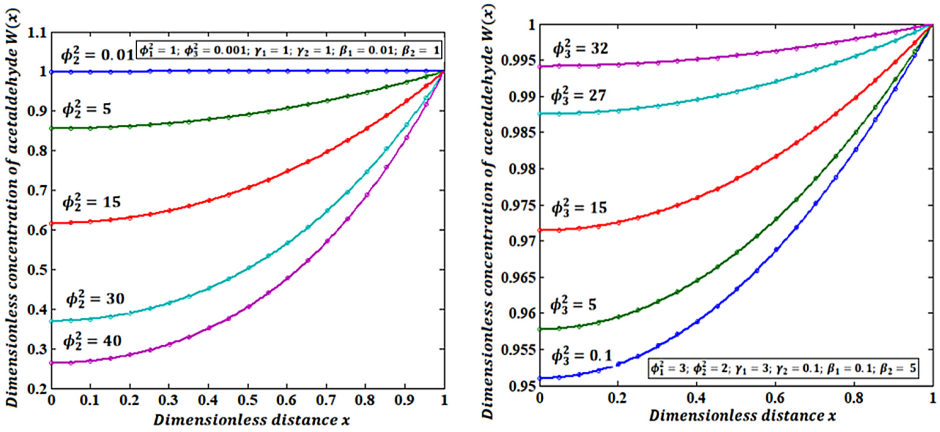

Figure 4: Comparison of numerical (dotted line) and analytical (solid line) results of the dimensionless concentration of ethanol $W(x)$ on the effect of ϕ_2^2 and ϕ_3^2.

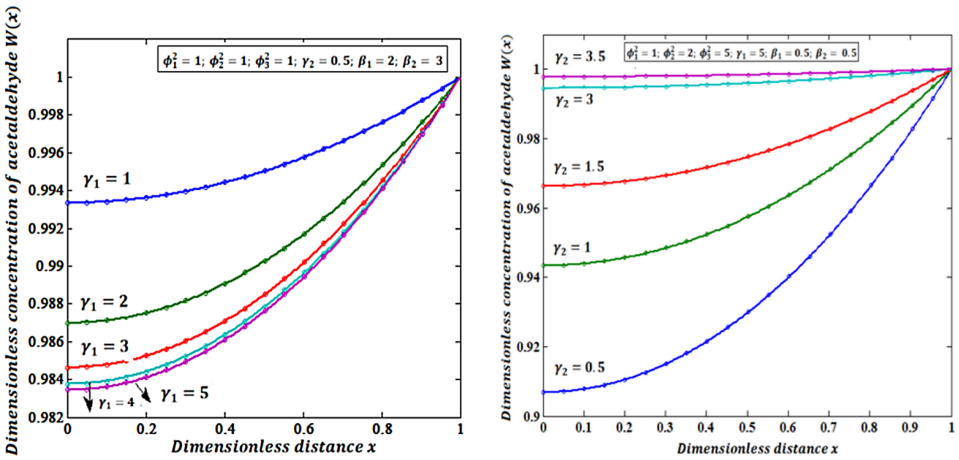

Figure 5: Comparison of numerical (dotted line) and analytical (solid line) results of the dimensionless concentration of ethanol $W(x)$ on the effect of γ_1 and γ_2.

the domain. Physically, this behavior indicates that larger γ_1 values intensify reaction or relaxation effects associated with acetaldehyde transport, thereby consuming or retarding the species within the boundary layer and reducing its concentration near the surface. In contrast, Figure 5(b) shows that increasing γ_2 enhances the acetaldehyde concentration profile. This suggests that γ_2 plays a supportive role in mass diffusion or species generation mechanisms, facilitating acetaldehyde transport and leading to higher concentration levels. In both subfigures, all profiles monotonically increase and satisfy the boundary condition at $x = 1$, ensuring physical consistency of the model. Figure 6 illustrates the effects of the parameters β_1 and β_2 on the dimensionless acetaldehyde concentration $W(x)$. Figure 6(a), increasing β_1 significantly enhances the concentration profile across the domain. Physically, this indicates that larger β_1 values strengthen mass diffusion or reduce the effective resistance to acetaldehyde transport, allowing the species to penetrate more efficiently from the surface into the fluid. At very small

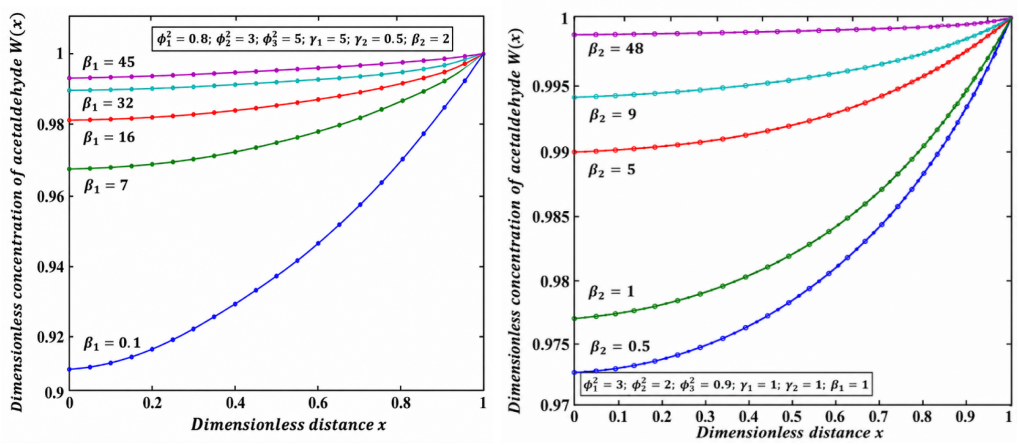

Figure 6: Comparison of numerical (dotted line) and analytical (solid line) results of the dimensionless concentration of acetaldehyde $W(x)$ on the effect of β_1 and β_2.

β_1, strong diffusion resistance suppresses $W(x)$, particularly near the wall region. Figure 6(b), a similar trend is observed with respect to β_2. Higher values of β_2 lead to elevated acetaldehyde concentration levels, suggesting that β_2 promotes diffusion or reaction mechanisms that support species transport within the boundary layer.

5.1 HFM superiority and limitations

HFM outperforms VIM and ADM by yielding compact, exact closed-form soliton solutions (e.g., sech/tanh profiles) for nonlinear PDEs like reaction-diffusion systems, requiring minimal term balancing versus VIM's iterative functionals or ADM's polynomial computations-thus achieving faster convergence with lower effort. However, HFM may fail for non-traveling wave problems, stiff equations needing high-order expansions, or systems lacking hyperbolic polynomial structures, where series methods provide better flexibility.

5.2 Molar concentrations of ethanol and acetaldehyde in the reaction stream

The variation of composition along the bed can be adequately described using the plug flow hypothesis [31]:

$$q_v \frac{dC_{Et}^b}{dm_{cat}} = -\frac{r_1\left(C_{Et}, C_{Ac}\right)}{\rho_{cat}}, \tag{20}$$

$$q_v \frac{dC_{Ac}^b}{dm_{cat}} = -\frac{\left(r_2\left(C_{Et}, C_{Ac}\right) - r_1\left(C_{Et}, C_{Ac}\right)\right)}{\rho_{cat}}. \tag{21}$$

Boundary conditions are:

$$m_{cat} = 0, \quad C_{Et}^b = C_{Et}^{b,0}, \quad C_{Ac}^b = 0. \tag{22}$$

For a reactor with uniform catalyst distribution, the relation between the catalyst mass coordinate and axial position is given by:

$$z = \frac{m_{cat}}{\rho_{cat} A_{bed}}, \tag{23}$$

where ρ_{cat} is the catalyst particle or bed density, A_{bed} is the bed's cross-sectional area, dz is the differential length increment along the axial direction.

The given rate equations (20) to (22), written in terms of the axial coordinate z, are:

$$q_v \frac{dC_{Et}^b(z)}{dz} = -k_{\text{ref},1} \frac{\exp\left[-\frac{E_1}{R_G}\left(\frac{1}{T}-\frac{1}{T_{\text{ref}}}\right)\right] C_{Et}(z)}{1+K_{C_{Et}}C_{Et}(z)+K_{C_{Ac}}C_{Ac}(z)} \rho_{\text{cat}} A_{\text{bed}}, \tag{24}$$

$$q_v \frac{dC_{Ac}^b}{dz} = \left\{ \begin{array}{c} -k_{\text{ref},2} \dfrac{\exp\left[-\frac{E_2}{R_G}\left(\frac{1}{T}-\frac{1}{T_{\text{ref}}}\right)\right] K_{C_{Ac}}C_{Ac}(z)}{1+K_{C_{Et}}C_{Et}(z)+K_{C_{Ac}}C_{Ac}(z)} \rho_{\text{cat}} A_{\text{bed}} \\ -k_{\text{ref},1} \dfrac{\exp\left[-\frac{E_1}{R_G}\left(\frac{1}{T}-\frac{1}{T_{\text{ref}}}\right)\right] C_{Et}(z)}{1+K_{C_{Et}}C_{Et}(z)+K_{C_{Ac}}C_{Ac}(z)} \rho_{\text{cat}} A_{\text{bed}} \end{array} \right\}, \tag{25}$$

where q_v is the volumetric flow rate. The boundary conditions are given as:

$$\text{At} \quad z=0: \quad C_{Et}^b = C_{Et}^{b,0}, \quad C_{Ac}^b = 0. \tag{26}$$

To nondimensionalize the system of Equations (24) to (26), the following substitutions are introduced:

$$\left\{ \begin{array}{l} u = \dfrac{C_{Et}^b}{C_{Et}^{b,0}}, \quad w = \dfrac{C_{Ac}^b}{C_{Et}^{b,0}}, \quad \xi = \dfrac{Z}{L}, \quad \varphi_1 = \dfrac{k_{\text{ref},1}\,\rho_{\text{cat}}\,A_{\text{bed}}\,R}{q_v}, \quad \varphi_2 = \dfrac{k_{\text{ref},2}\,\rho_{\text{cat}}\,A_{\text{bed}}\,R}{q_v}, \\ \sigma_1 = K_{C_{Et}}C_{Et}^{b,0}, \quad \sigma_2 = K_{C_{Ac}}C_{Et}^{b,0}, \quad \gamma_1 = \dfrac{E_1}{R_G}\left(\dfrac{1}{T}-\dfrac{1}{T_{\text{ref}}}\right), \quad \gamma_2 = \dfrac{E_2}{R_G}\left(\dfrac{1}{T}-\dfrac{1}{T_{\text{ref}}}\right). \end{array} \right. \tag{27}$$

Using the dimensionless variables (27) Equations (24) and (25) are transformed into

$$\frac{du(\xi)}{d\xi} = -\varphi_1 e^{-\gamma_1} \frac{u(\xi)}{1+\sigma_1 u(\xi)+\sigma_2 w(\xi)}, \tag{28}$$

$$\frac{dw(\xi)}{d\xi} = \varphi_1 e^{-\gamma_1} \frac{u(\xi)}{1+\sigma_1 u(\xi)+\sigma_2 w(\xi)} - \varphi_2 e^{-\gamma_2} \frac{\sigma_2 w(\xi)}{1+\sigma_1 u(\xi)+\sigma_2 w(\xi)}. \tag{29}$$

Dimensionless boundary conditions are in the forms:

$$u(0)=1, \quad w(0)=0. \tag{30}$$

Because Equations (28) and (29) are difficult to solve directly, we have instead focused on analysing the following limiting cases.

5.2.1 Limiting cases for molar concentrations of ethanol and acetaldehyde in the reaction stream:

Case 1: Arbitrary σ_1 (product does not inhibit via w)

The Equations (28) and (29) become,

$$\frac{du(\xi)}{d\xi} = -\varphi_1 e^{-\gamma_1} \frac{u(\xi)}{1+\sigma_1 u(\xi)}, \quad \text{and} \quad \frac{dw(\xi)}{d\xi} = \varphi_1 e^{-\gamma_1} \frac{u(\xi)}{1+\sigma_1 u(\xi)}. \tag{31}$$

On solving the Equation (31) with the boundary condition (30) we obtain:

$$u(\xi) = \frac{1}{\sigma_1} W\left(\sigma_1 e^{\sigma_1 - \varphi_1 e^{-\gamma_1}\xi}\right), \quad \text{and} \quad w(\xi) = 1-u(\xi) = 1-\frac{1}{\sigma_1} W\left(\sigma_1 e^{\sigma_1 - \varphi_1 e^{-\gamma_1}\xi}\right), \tag{32}$$

where $W(x)$ is Lambert W-function. The Lambert W-function physically represents the balance in systems where a variable appears both linearly and inside an exponential, capturing self-consistent exponential feedback. It extracts the true state of processes governed by coupled growth/decay and constraint, common in kinetics, transport, and activation phenomena.

Case 2: Small $u(\xi), w(\xi)$ $(\sigma_1 u, \sigma_2 w \ll 1)$

The Equations (28) and (29) become,

$$\frac{du(\xi)}{d\xi} = \varphi_1 e^{-\gamma_1} u(\xi), \quad \text{and} \quad \frac{dw(\xi)}{d\xi} = \varphi_1 e^{-\gamma_1} u(\xi) - \varphi_2 e^{-\gamma_2} \sigma_2 w(\xi). \tag{33}$$

On solving the above equation with the corresponding initial condition, we obtain the result as:

$$u(\xi) = e^{-\varphi_1 e^{-\gamma_1} \xi}, \quad \text{and} \quad w(\xi) = \frac{\varphi_1 e^{-\gamma_1}}{\varphi_2 e^{-\gamma_2} \sigma_2 - \varphi_1 e^{-\gamma_1}} \left[e^{-\varphi_1 e^{-\gamma_1} \xi} - e^{-\varphi_2 e^{-\gamma_2} \sigma_2 \xi} \right]. \tag{34}$$

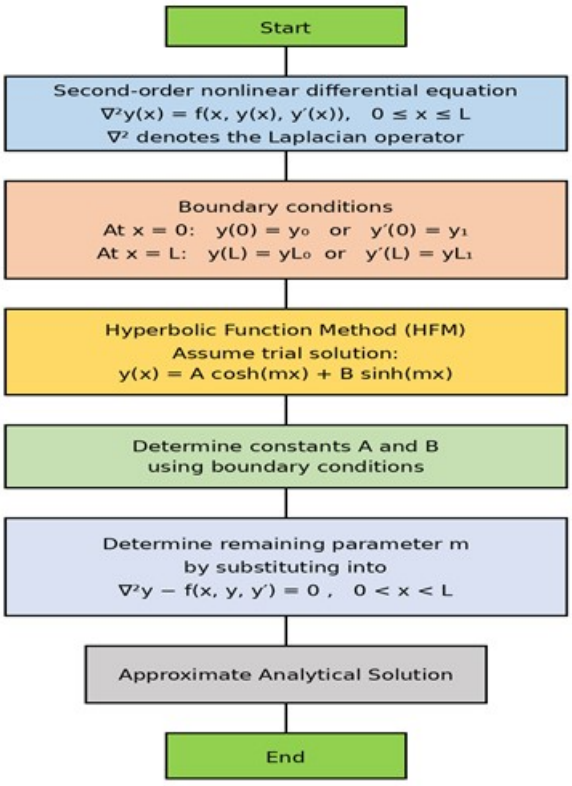

Figure 7: Flowchart of the solution methodology (HFM).

6 Conclusion

The research establishes that the hyperbolic function method is a robust and efficient strategy for simulating nonlinear catalytic combustion phenomena within fixed-bed reactors, notably

regarding ethanol oxidation on a Mn_9Cu_1 catalyst. MATLAB-based numerical validations confirm that this semi-analytical approach accurately encompasses both transport and reaction kinetics, delivering solutions that are not only precise but also computationally cost-effective. This capability enhances reactor performance analysis and catalyst optimization, paving the way for significant advances in fuel oxidation technology and catalytic process engineering.

Appendix A: Solution of nonlinear equations (7) and (8) using the HFM and flowchart of the solution methodology

The nonlinear differential Equations (7) and (8) can be expressed in the following form:

$$U''(x) + \frac{2}{x}U'(x) = \phi_1^2 e^{-\gamma_1} f_1(U(x), W(x)), \tag{35}$$

$$W''(x) + \frac{2}{x}W'(x) = \phi_2^2 e^{-\gamma_2} f_2(U(x), W(x)) - \phi_3^2 e^{-\gamma_1} f_1(U(x), W(x)), \tag{36}$$

subject to the boundary conditions:

$$\text{At} \quad x = 0: \quad \frac{dU}{dx} = 0, \quad \frac{dW}{dx} = 0, \tag{37}$$

$$\text{At} \quad x = 1: \quad U = 1, \quad W = 1. \tag{38}$$

Here, the nonlinear functions $f_1(U, W)$ and $f_2(U, W)$ are defined as:

$$f_1(U, W) = \frac{U}{1 + \beta_1 U + \beta_2 W}, \quad f_2(U, W) = \frac{W}{1 + \beta_1 U + \beta_2 W}.$$

To obtain an approximate analytical form of the solution for Equations (7) and (8), the functions $U(x)$ and $W(x)$ are assumed to follow the hyperbolic structure:

$$U(x) = A\cosh(mx) + B\sinh(mx), \tag{39}$$

$$W(x) = C\cosh(nx) + D\sinh(nx), \tag{40}$$

where A, B, C, D, m, and n are constants to be determined. Applying the boundary conditions (37) and (38) to Equations (39) and (40), the constants are evaluated as:

$$A = \frac{1}{\cosh(m)}, \quad B = 0, \quad C = \frac{1}{\cosh(n)}, \quad D = 0. \tag{41}$$

Thus, Equations (39) and (40) simplify to:

$$U(x) = \frac{\cosh(mx)}{\cosh(m)}, \tag{42}$$

$$W(x) = \frac{\cosh(nx)}{\cosh(n)}. \tag{43}$$

Substituting Equations (42) and (43) into the governing Equations (35) and (36) yields:

$$m^2 \frac{\cosh(mx)}{\cosh(m)} + \frac{2}{x}\frac{m\sinh(mx)}{\cosh(m)} = \phi_1^2 e^{-\gamma_1} \left[\frac{\frac{\cosh(mx)}{\cosh(m)}}{1 + \beta_1 \left(\frac{\cosh(mx)}{\cosh(m)}\right) + \beta_2 \left(\frac{\cosh(nx)}{\cosh(n)}\right)} \right], \tag{44}$$

$$n^2\frac{\cosh(nx)}{\cosh(n)}+\frac{2}{x}\frac{n\sinh(nx)}{\cosh(n)}=\phi_2^2e^{-\gamma_2}\left[\frac{\frac{\cosh(nx)}{\cosh(n)}}{1+\beta_1\left(\frac{\cosh(mx)}{\cosh(m)}\right)+\beta_2\left(\frac{\cosh(nx)}{\cosh(n)}\right)}\right]$$
$$-\phi_3^2e^{-\gamma_1}\left[\frac{\frac{\cosh(mx)}{\cosh(m)}}{1+\beta_1\left(\frac{\cosh(mx)}{\cosh(m)}\right)+\beta_2\left(\frac{\cosh(nx)}{\cosh(n)}\right)}\right]. \tag{45}$$

At $x=0$, these equations reduce to the following simplified relationships:

$$\frac{m^2}{\cosh(m)}+\frac{2m^2}{\cosh(m)}=\phi_1^2e^{-\gamma_1}\left[\frac{\frac{1}{\cosh(m)}}{1+\beta_1\left(\frac{1}{\cosh(m)}\right)+\beta_2\left(\frac{1}{\cosh(n)}\right)}\right], \tag{46}$$

$$\frac{n^2}{\cosh(n)}+\frac{2n^2}{\cosh(n)}=\phi_2^2e^{-\gamma_2}\left[\frac{\frac{1}{\cosh(n)}}{1+\beta_1\left(\frac{1}{\cosh(m)}\right)+\beta_2\left(\frac{1}{\cosh(n)}\right)}\right]$$
$$-\phi_3^2e^{-\gamma_1}\left[\frac{\frac{1}{\cosh(m)}}{1+\beta_1\left(\frac{1}{\cosh(m)}\right)+\beta_2\left(\frac{1}{\cosh(n)}\right)}\right]. \tag{47}$$

On simplifying above equations we get,

$$\frac{3m^2}{\cosh(m)}=\frac{\phi_1^2e^{-\gamma_1}\cosh(n)}{\cosh(n)\left(\cosh(m)+\beta_1\right)+\beta_2\cosh(m)}, \tag{48}$$

$$\frac{3n^2}{\cosh(n)}=\frac{\phi_2^2e^{-\gamma_2}\cosh(m)-\phi_3^2e^{-\gamma_1}\cosh(n)}{\cosh(n)\left(\cosh(m)+\beta_1\right)+\beta_2\cosh(m)}. \tag{49}$$

Equations (48) and (49) form a coupled nonlinear algebraic system in the unknowns m and n. These parameters are obtained by solving the system numerically using computational tools such as Wolfram Alpha, MATLAB, or Python, for selected parameter values of ϕ_1^2, ϕ_2^2, $\phi_3^2, \gamma_1, \gamma_2, \beta_1$, and β_2.

The corresponding values of m and n are then substituted into Equations (42) and (43) to reconstruct the approximate analytical expressions for $U(x)$ and $W(x)$, which characterize the nonlinear coupled response of the system. The HFM provides an efficient semi-analytical framework for solving the nonlinear coupled equations under consideration. Hyperbolic function approximations enable this method to accurately capture the system's key nonlinear dynamics and parameter sensitivities using fewer iterations and minimal computational resources. Furthermore, the method offers clear physical insight into the influence of governing parameters, making it particularly valuable for analysing nonlinear transport and interaction phenomena in complex systems.

Appendix B: Matlab program to solve the nonlinear Equations (7) and (8)

```
function bvp_AB_solver

    % Parameters (fixed)
    alpha2 = 1;
    alpha3 = 1;
```

```
    deltal = 2.5;
    delta2 = 0.5;
    lambda1 = 1;
    lambda2 = 1;
    % Varying alpha1
    alpha1_vals = [1];
    colors = lines(length(alpha1_vals));
    figure; hold on;
    legend_entries = {};
    for i=1:length(alpha1_vals)
        alpha1 = alpha1_vals(i);
        params = [alpha1, alpha2, alpha3, delta1, delta2, lambda1, lambda2];


        % Initial mesh
        solinit = bvpinit(linspace(1e-4, 1, 100), @ guess);
        sol = bvp4c(@(xi, y) odefun(xi, y, params), @ bcfun, solinit);
        xi = linspace(1e-4, 1, 200);
        Y= deval(sol, xi);
        % Plot A(xi) with line and dots
        plot(xi, Y(1,:), '-', 'Color', colors(i,:), 'LineWidth', 1.5);
        plot(xi(1:10:end), Y(1,1:10:end), 'o', 'Color', colors(i,:), 'MarkerSize', 4);
        legend_entries {end+1} = ['\alpha_1 = ', num2str(alpha1)];
    end
    xlabel('\xi');
    ylabel('A(\xi)');
    title('Variation of A(\xi) with different \alpha_1');
    legend(legend_entries, 'Location', 'best');
    grid on;
end

% ---- ODE System ----
function dydx = odefun(xi, y, p)
    % y = [A; A'; B; B']
    A = y(1);
    dA = y(2);
    B=y(3);
    dB = y(4);

    % Unpack parameters
    alpha1 = p(1);
    alpha2 = p(2);
    alpha3 = p(3);
    deltal = p(4);
    delta2 = p(5);
    lambda1 = p(6);
    lambda2 = p(7);
    denom = 1 + lambda1*A + lambda2*B;
    G1 = alpha1 * exp(-delta1) * A / denom;
    G2 = alpha2 * exp(-delta2) * B / denom - alpha3 * exp(-delta1) * A / denom;
    dydx = zeros(4,1);
    dydx(1)= dA;
    dydx(2) = -2/xi * dA+G1;
    dydx(3)=dB;
    dydx(4)= -2/xi * dB + G2;
end

% ---- Boundary Conditions ----
function res = bcfun(ya, yb)

     % ya and yb correspond to y at xi=0 and xi=1
```

```
    res = [ya(2);    % dA/dxi at xi=0
         ya(4);    % dB/dxi at xi=0
         yb(1) - 1;    % A(1) = 1
         yb(3) - 1];    % B(1) = 1

end

% ---- Initial Guess ----
function g = guess(x)
  g = [1; 0; 1; 0]; % A, dA, B, dB
end
```

Nomenclature

C_{Et}	Molar concentration of ethanol inside the catalyst particle ($\mathrm{mol/m^3}$)
C_{Ac}	Molar concentration of acetaldehyde inside the catalyst particle $\left(\mathrm{mol/m^3}\right)$
C_{Et}^{b}	Bulk molar concentration of ethanol ($\mathrm{mol/m^3}$)
C_{Ac}^{b}	Bulk molar concentration of acetaldehyde ($\mathrm{mol/m^3}$)
$C_{Et}^{b,0}$	Initial bulk molar concentration of ethanol (mol/m^3)
$D_{\mathrm{ef},Et}$	Effective diffusivity of ethanol ($\mathrm{m^2/s}$)
$D_{\mathrm{ef},Ac}$	Effective diffusivity of acetaldehyde ($\mathrm{m^2/s}$)
R	Radius of catalyst particle (m)
z	Axial coordinate in particle/reactor (m)
$x = \frac{z}{R}$	Dimensionless axial coordinate inside particle
$\xi = \frac{z}{L}$	Dimensionless axial coordinate along bed
q_v	Volumetric flow rate ($\mathrm{m^3/s}$)
ρ_{cat}	Catalyst particle density ($\mathrm{kg/m^3}$)
A_{bed}	Cross-sectional area of the bed ($\mathrm{m^2}$)
$k_{\mathrm{ref},1}$	Pre-exponential factor for ethanol reaction (1/s)
$k_{\mathrm{ref},2}$	Pre-exponential factor for acetaldehyde reaction (1/s)
E_1	Activation energy for ethanol reaction (J/mol)
E_2	Activation energy for acetaldehyde reaction (J/mol)
r_1	Reaction rate of ethanol consumption ($\mathrm{mol/}\left(\mathrm{m^3 \cdot\ s}\right)$)
r_2	Reaction rate of acetaldehyde formation ($\mathrm{mol/}\left(\mathrm{m^3 \cdot\ s}\right)$)
$r_{obs,1}, r_{obs,2}$	Observed reaction rates in reactor ($\mathrm{mol/}\left(\mathrm{m^3 \cdot\ s}\right)$)
$K_{C_{Et}}$	Adsorption equilibrium constant for ethanol ($\mathrm{m^3/mol}$)
$K_{C_{Ac}}$	Adsorption equilibrium constant for acetaldehyde ($\mathrm{m^3/mol}$)

T	Operating temperature (K)
T_{ref}	Reference temperature (K)
R_G	Universal gas constant (J/(mol•K))
$U = \frac{C_{Et}}{C^b_{Et}}$	Dimensionless ethanol concentration inside particle
$W = \frac{C_{Ac}}{C^b_{Ac}}$	Dimensionless acetaldehyde concentration inside particle
$u = \frac{C^b_{Et}}{C^{b,0}_{Et}}$	Dimensionless bulk ethanol concentration along bed
$w = \frac{c^b_{Ac}}{c^{b,0}_{Et}}$	Dimensionless bulk acetaldehyde concentration along bed
$\phi_1^2 = \frac{k_{\text{ref},1} R^2}{D_{\text{ef},Et}}$	Thiele modulus for ethanol
$\phi_2^2 = \frac{k_{\text{ref},2} R^2}{D_{\text{ef},Et}}$	Thiele modulus for acetaldehyde
$\phi_3^2 = \frac{k_{\text{ref},1} c^b_{Et} R^2}{D_{\text{ef},Ac} c^b_{Ac}}$	Coupling parameter
$\beta_1 = K_{C_{Et}} C^b_{Et}$	Dimensionless adsorption parameter for ethanol
$\beta_2 = K_{C_{Ac}} C^b_{Ac}$	Dimensionless adsorption parameter for acetaldehyde
$\gamma_1 = \frac{E_1}{R_G}\left(\frac{1}{T} - \frac{1}{T_{\text{ref}}}\right)$	Dimensionless activation energy for ethanol
$\gamma_2 = \frac{E_2}{R_G}\left(\frac{1}{T} - \frac{1}{T_{\text{ref}}}\right)$	Dimensionless activation energy for acetaldehyde
$\varphi_1 = \frac{k_{\text{ref},1} \rho_{\text{cat}}\ A_{\text{bed}}\ R}{q_v}$	Dimensionless reaction parameter for ethanol along bed
$\varphi_2 = \frac{k_{\text{ref},2} \rho_{\text{cat}}\ A_{\text{bed}}\ R}{q_v}$	Dimensionless reaction parameter for acetaldehyde along bed
$\sigma_1 = K_{C_{Et}} C^{b,0}_{Et}$	Dimensionless adsorption parameter along bed for ethanol
$\sigma_2 = K_{C_{Ac}} C^{b,0}_{Et}$	Dimensionless adsorption parameter along bed for acetaldehyde

Conflicts of Interest. The authors declare that they have no conflicts of interest regarding the publication of this article.

References

[1] J. Mittal, Recent progress in the synthesis of layered double hydroxides and their application for the adsorptive removal of dyes: a review, *J. Environ. Manage.* **295** (2021) #113017, https://doi.org/10.1016/j.jenvman.2021.113017.

[2] R. Okabe, A. Miura, M. Fukushima, M. Terashima, M. Sasaki, S. Fukuchi and T. Sato, Characterization of an adsorbed humin-like substance on an allophanic

soil formed via catalytic polycondensation between catechol and glycine and its adsorption capability toward pentachlorophenol, *Chemosphere* **83** (2011) 1502–1506, https://doi.org/10.1016/j.chemosphere.2011.01.053.

[3] J. -Y. Chin and S. A. Batterman, VOC composition of current motor vehicle fuels and vapors and collinearity analyses for receptor modeling, *Chemosphere* **86** (2012) 951–958, https://doi.org/10.1016/j.chemosphere.2011.11.017.

[4] G. Rochard, L. Olivet, M. Tannous, C. Poupin, S. Siffert and R. Cousin, Recent advances in the catalytic treatment of volatile organic compounds: a review based on the mixture effect, *Catalysts* **11** (2021) #1218, https://doi.org/10.3390/catal11101218.

[5] M. J. M. Figueredo, C. Cocuzza, S. Bensaid, D. Fino, M. Piumetti and N. Russo, Catalytic abatement of volatile organic compounds and soot over manganese oxide catalysts, *Materials* **14** (2021) #4534, https://doi.org/10.3390/ma14164534.

[6] E. Loccufier, G. Watson, Y. Zhao, M. Meledina, R. Denis, P. G. Derakhshandeh, P. V. D. Voort, K. Leus, D. P. Debecker, K. D. Buysser and K. D. Clerck, CO2 methanation with Ru@MIL-101 nanoparticles fixated on silica nanofibrous veils as standalone structured catalytic carriers, *Appl. Catal. B: Environ.* **320** (2023) #121972, https://doi.org/10.1016/j.apcatb.2022.121972.

[7] C. He, J. Cheng, X. Zhang, M. Douthwaite, S. Pattisson and Z. Hao, Recent advances in the catalytic oxidation of volatile organic compounds: a review based on pollutant sorts and sources, *Chem. Rev.* **119** (2019) 4471–4568, https://doi.org/10.1021/acs.chemrev.8b00408.

[8] D. F. de Waard, P. D. Kouris, M. D. Boot and E. J. M. Hensen, Mixed Cu–Mn oxide catalysts for solvolysis of technical lignin, *ACS Sustainable Chem. Eng.* **13** (2025) 3269–3279, https://doi.org/10.1021/acssuschemeng.4c09666.

[9] X. Zha, C. Yang, X. Huang, J. Ding and Z. Ding, Recent progress and perspectives on metal oxide catalysts for thermocatalytic and photocatalytic oxidation of VOCs: a review, *Environ. Pollut. Bioavailab.* **36** (2024) #2376827, https://doi.org/10.1080/26395940.2024.2376827.

[10] M. K. Zamisa, T. W. Seadira and S. J. Baloyi, Transforming wastewater treatment: Recent advancements in catalytic wet air oxidation with pillared clay catalysts for phenol remediation, *Environ. Pollut.* **361** (2024) #124842, https://doi.org/10.1016/j.envpol.2024.124842.

[11] M. L. Rodriguez and L. E. Cadus, Mass transfer limitations in a monolithic reactor for the catalytic oxidation of ethanol, *Chem. Eng. Sci.* **143** (2016) 305–313, https://doi.org/10.1016/j.ces.2015.12.010.

[12] P. O. Larsson and A. Andersson, Oxides of copper, ceria-promoted copper, manganese, and copper–manganese on Al2O3 for the combustion of CO, ethyl acetate, and ethanol, *Appl. Catal. B: Environ.* **24** (2000) 175–192, https://doi.org/10.1016/S0926-3373(99)00104-6.

[13] D. Z. Khater, R. S. Amin, M. Mahmoud and K. M. El-Khatib, Evaluation of mixed transition-metal (Co, Mn, and Cu) oxide electrocatalysts anchored on different carbon supports for robust oxygen reduction reaction in neutral media, *RSC Adv.* **12** (2022) 2207–2218, https://doi.org/10.1039/d1ra07721j.

[14] D. Delimaris and T. Ioannides, VOC oxidation over $MnO_x - CeO_2$ catalysts prepared by a combustion method, *Appl. Catal. B: Environ.* **84** (2008) 303–312, https://doi.org/10.1016/j.apcatb.2008.04.006.

[15] T. Liu, Y. Yao, L. Wei, Z. Shi, L. Han, H. Yuan, B. Li, L. Dong, F. Wang and C. Sun, Preparation and evaluation of copper–manganese oxide as a high-efficiency catalyst for CO oxidation and NO reduction by CO, *J. Phys. Chem. C* **121** (2017) 12757–12770, https://doi.org/10.1021/acs.jpcc.7b02052.

[16] M. Dehghan and J. Manafian, The solution of variable-coefficient fourth-order parabolic partial differential equations by the homotopy perturbation method, *Z. Naturforsch. A* **64** (2009) 420–430.

[17] M. Dehghan, J. Manafian and A. Saadatmandi, Solving nonlinear fractional partial differential equations using the homotopy analysis method, *Numer. Methods Partial Differential Equations* **26** (2010) 448–479.

[18] M. Izadi, S. K. Yadav and G. Methi, Two efficient numerical techniques for solutions of fractional shallow water equation, *Partial Differ. Equ. Appl. Math.* **9** (2024) #100619, https://doi.org/10.1016/j.padiff.2024.100619.

[19] M. Dehghan, J. Manafian and A. Saadatmandi, Application of semi-analytical methods for solving the Rosenau-Hyman equation arising in the pattern formation in liquid drops, *Internat. J. Numer. Methods Heat Fluid Flow* **22** (2012) 777–790, https://doi.org/10.1108/09615531211244916.

[20] R. Rajalakshmi, A. Marimuthu, S. Naganathan, L. Rajendran and M. Izadi, Mathematical modeling and sensitivity analysis of enzymatic biofuel cells with various electrode geometries, *J. Appl. Comput. Mech.* (2025) In Press, https://doi.org/10.22055/jacm.2025.48646.5391.

[21] Y. Qian, J. Manafian, S. Y. Mohyaldeen, L. S. Esmail, S. A. Gorovoy and G. Singh, Multiple-order line rogue wave, lump and its interaction, periodic, and cross-kink solutions for the generalized CHKP equation, *Propuls. Power Res.* **10** (2021) 277–293, https://doi.org/10.1016/j.jppr.2021.09.002.

[22] Y. F. Patel and M. Izadi, Dynamic modeling and parameter sensitivity in singular non-isothermal reaction-diffusion systems: A DTM-Padé solution for spherical catalysts, *J. Nonlinear Math. Phys.* **32** (2025) #71, https://doi.org/10.1007/s44198-025-00332-2.

[23] P. Zhou, J. Manafian, M. Lakestani, O. A. Ilhan, N. J. angi Bahador, A. A. Fattah, K. H. Mahmoud, R. Nuray and N. Nagiyeva, Analytical evaluations using a neural-network-based method for wave solutions of the combined Kairat-II-X differential equation in fluid mechanics, *Sci. Rep.* **16** (2026) #7753, https://doi.org/10.1038/s41598-026-38761-8.

[24] M. S. Dahaghin and H. Hassani, A new optimization method for a class of time-fractional convection–diffusion–wave equations with variable coefficients, *Eur. Phys. J. Plus.* **132** (2017) #130, https://doi.org/10.1140/epjp/i2017-11407-y.

[25] H. Hassani, Z. Avazzadeh, P. Agarwal, M. J. Ebadi and A. Bayati Eshkaftaki, Generalized Bernoulli–Laguerre polynomials: Applications in coupled nonlinear systems of variable-order fractional PDEs, *J. Optim. Theory Appl.* **200** (2024) 371–393, https://doi.org/10.1007/s10957-023-02346-6.

[26] S. Sabermahani, Y. Ordokhani and H. Hassani, General Lagrange scaling functions: Application in a general model of variable-order fractional partial differential equations, *Comput. Appl. Math.* **40** (2021) #269.

[27] Z. Avazzadeh and H. Hassani, Transcendental Bernstein series for solving reaction–diffusion equations with nonlocal boundary conditions through an optimization technique, *Numer. Methods Partial Differential Equations* **35** (2019) 2258–2274, https://doi.org/10.1002/num.22411.

[28] A. Ghasemi and A. Saadatmandi, A Bernoulli-reproducing kernel method for a class of nonlinear singular boundary value problems, *J. Appl. Anal. Comput.* **14** (2024) 3260–3281, https://doi.org/10.11948/20230508.

[29] M. Izadi, H. Ahmad and H. M. Srivastava, Numerical computations of time-dependent auto-catalytic glycolysis chemical reaction-diffusion system, *MATCH Commun. Math. Comput. Chem.* **93** (2025) 69–97, https://doi.org/10.46793/match.93-1.069I.

[30] R. Nalini, A. Meena, L. Rajendran and M. Izadi, Approximate solutions of transient reaction-diffusion equations for second-order regeneration at spherical microelectrodes via HPM, *Edelweiss Appl. Sci. Technol.* **9** (2025) 1471–1483, https://doi.org/10.55214/2576-8484.v9i9.10155.

[31] M. Agustina Campesi, N. J. Mariani, M. C. Pramparo, B. P. Barbero, L. E. Cadús, O. M. Martínez and G. F. Barreto, Combustion of volatile organic compounds on a MnCu catalyst: A kinetic study, *Catal. Today* **176** (2011) 225–228, https://doi.org/10.1016/j.cattod.2011.01.009.

[32] M. L. Clarance Mary, M. Chitra Devi, A. Meena, L. Rajendran and M. Abukhaled, A reliable Taylor series solution to the nonlinear reaction–diffusion model representing the steady-state behavior of a cationic glucose-sensitive membrane, *J. Math. Comput. Sci.* **11** (2021) 8354–8381, https://doi.org/10.28919/jmcs/6799.

[33] M. Chitra Devi, P. Pirabaharan, L. Rajendran and M. Abukhaled, An efficient method for finding analytical expressions of substrate concentrations for different particles in an immobilized enzyme system, *Reac. Kinet. Mech. Cat.* **130** (2020) 35–53, https://doi.org/10.1007/s11144-020-01757-0.

[34] M. Chitra Devi, P. Pirabaharan, M. Abukhaled and L. Rajendran, Analysis of the steady-state behavior of a pseudo-first-order EC-catalytic mechanism at a rotating disk electrode, *Electrochim. Acta* **345** (2020) #136175, https://doi.org/10.1016/j.electacta.2020.136175.

[35] K. M. Dharmalingam, M. Veeramuni and K. Valli, Ethanol and acetaldehyde in a fixed-bed laboratory reactor by the Adomian decomposition method, *Malaya J. Mat.* **8** (2020) 886–892, https://doi.org/10.26637/MJM0803/0026.

[36] K. M. Dharmalingam, M. Veeramuni, H. Rezazadeh, C. Tunç, Variational iteration method for solving ethanol and acetaldehyde concentrations in a fixed-bed laboratory reactor, *Appl. Appl. Math.* **16** (2021) 383–398.